

Research Article

Design and Analysis of Shear Pin of Lever Arm in Generator Circuit Breaker Using Finite Element Method

K. Jaiyen

W. Rangsi*

Department of Mechanical
Engineering, Faculty of Engineering,
Chiang Mai University, Chiang Mai,
50200, Thailand

Received 15 September 2023

Revised 9 December 2023

Accepted 19 December 2023

Abstract:

Interruption in mechanism of the generator circuit breaker is a main cause of an overload impact and fracture of lever arm, resulting in suspension of the power plant's electricity transmission. Recently, shear pin has gained more interest owing to its ability to be a force-transmitting and break-away parts. Herein, finite element simulation analysis was investigated using Abaqus explicit software. Three-dimensional (3D) model of the lever arm and clevis pin were simulated based on actual dimension and velocity for analysing stress and force between the lever arm and pin due to impact. Notch and hollow pins with different shear cross-sectional areas were also simulated using the similar model. Deformation, energy dissipation, and failure load of various shear pin dimensions were investigated to yield the suitable shear pin for preventing lever arm's fracture. The great potential notch pin with 6 mm in-depth to protect the lever arm from damages could be assumed.

Keywords: Crank arm, Impact analysis, Numerical simulation, Power plant, Shear bolt, Failure

1. Introduction

The suspension of electricity supply from a hydroelectric power plant to the transmission line, leading to the shutdown of the power plant, is primarily attributed to the interruption in the generator circuit breaker. This breaker plays a main role in the closing-opening circuit of the power plant. Following the inspection, the damaged lever arm, an important part of the breaker mechanism, is a critical factor in the unsuccessful electricity transmission (Fig. 1a). The overall operational functions of the circuit breaker (Fig. 1b) can be categorized into two functions, i.e. opening and closing circuit [1]. The closing circuit mechanisms are explained as follows [2]; (i) prior to initiating the closing circuit phase, the closing spring is preloaded in a compressed state to store energy, (ii) the closing spring is extended, resulting in a 60-degree clockwise rotation of the lever arm, and push up the tie rod for electrical circuit connection, and (iii) the opening spring is compressed for energy storage. The opening circuit mechanisms start as follows; (i) the opening spring, previously compressed during the closing circuit sequence, will be extended, resulting in a 60-degree counterclockwise rotation of the lever arm and pulling down the tie rod, and (ii) the electrical circuit is then immediately separated within 20 ms to complete the opening circuit. To decelerate the motion and prevent impact on the internal parts within the breaker mechanism, the lever arm's end-point is mounted with oil dashpot. Nevertheless, if there is a malfunction of the oil dashpot, it can lead to the fracture of the end-point of the lever arm, which is the highest stress concentration area [3, 4]. In this case, power plants will lose an opportunity to generate electricity.

* Corresponding author: W. Rangsi
E-mail address: w.rangsi@gmail.com



Replacement of the lever arm has been reported as a traditional solution to address this issue. However, a significant drawback arises from the scarcity of available spare lever arms. Consequently, fixing the fracture in the level arm remains a critical and challenging task and needs more attention.

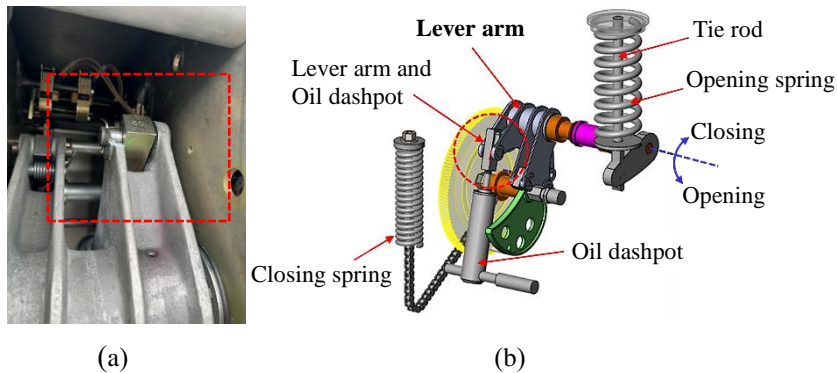


Fig. 1. (a) The lever arm fracture location and (b) the assembly of moving parts inside the breaker.

Recently, shear pins have gained more interest as a promising alternative device due to their ability to serve as a sacrificial part engineered for emergency break-away to protect other parts from being damaged in case of mechanical overload [5]. The shear pin in this regard is thus expected to be used instead of the clevis pin on the lever arm's end-point. It will function as a force-transmitting part under normal conditions and break instead of the lever arm in case of overload impact force. According to the literature, the design and analysis of stress and fracture on the pin from being sheared by using the finite element method are reported [5-11]. For example, Budiman et al. [6] investigated the shear pin protecting a guide vane in a Francis-type hydro turbine under various loading scenarios by using finite element and computational fluid dynamics. Sankar et al. [7] revealed the root cause of the failure of shear pins in a wind turbine generator. Kiran Kumar et al. [5] reported the shear strength of the shear pin material in aero engines by using finite element analysis. Yu et al. [8] found the influence of the diameter-thickness ratio on the failure mode and load of the civil aircraft pylon fuse pin by using the finite element simulation model Abaqus. Hiremath et al. [9] studied the fracture characteristics of hollow shear pins in aerospace applications. Zhang et al. [10] revealed the influence of the strain rate and damage parameters on the fuse pin strength and emergency separation in civilian aircraft during wheel-up crash landing by using the nonlinear explicit solver Abaqus/Explicit. Jin et al. [11] mainly evaluated the shear fracture and failure process of the hollow shear pin installed on the aircraft engine pylon through a 3D finite element method.

This research investigated the design concepts of the lever arm's shear pin in terms of dimensional design rather than material strength design. The shear pin requires no damage within an allowable load range. However, the shear pin was damaged under specifically certain load conditions. Thus, the assigned limits of the failure load of the shear pin were highly required. Therefore, the non-linear finite element method was applied into two parts. Firstly, the impact simulation of the lever arm with an existing clevis pin for analyzing contact force between hole of level arm and clevis pin was simulated. The analyzed contact force was assigned as the failure load of shear pin. Then the fracture process of the shear pin was simulated using the similar finite element model, but existing clevis pin was replaced by the notch pin and hollow pin with different notch depths and inner hole diameters. The influence of different notch depths and inner hole diameters on the strength and failure load of the shear pins with each configuration were analyzed. This research could provide experimental basis for the analysis and selection of suitable dimension of the shear pin for protecting fracture of the lever arm.

2. Experimental Setup

The shear pin assembled on the lever arm of the circuit breaker was designed in this research with an expected function as a sacrificial part to protect the lever arm when there is a malfunction in the circuit breaker mechanism. To design the shear pin as an emergency break-away part, the strength and dynamic characteristics are crucial factors, which require both a definite lower and an upper limit of strength. Finite element analysis (FEA) was conducted based on an impact simulation using Abaqus explicit finite element software, which analyzes the impact loading on the lever arm to collect strength limits of shear pins. Then, the fracture analysis of the shear pin was studied using a similar finite element model, which replaced the existing clevis pin with 2 types of shear pins.

2.1 Geometry and Structure

To simulate the impact load on the lever arm, the entire model as well as the fracture and failure of local structures were simulated and analyzed. The created 3D assembly model consisted of the lever arm, clevis pin, and stopper bar. The 3D model of the fractured region of the lever arm with a complicated shape, which aimed to analyze stress created by an undamaged lever arm to measure in three dimensions with a Faro edge portable coordinate measurement machine. The model of the clevis pin with an outside diameter of 20 mm, which was equal to the fitting hole at the end of the lever arm, was established. The stopper bar was built to be as a rectangular, corresponding to the actual dimension to the top part of the oil dash-pot. Finally, all 3D models were created into a 3D shape using the commercial software Solidworks, and were exported as Parasolid files to be used for analysis with Abaqus finite element software. The 3D models are shown in Fig. 2.

The prime aspect of the current work is to study the substitutability of an existing clevis pin with new shear pin. Thus, it is essential to reduce the failure load of the clevis pin by decreasing the resisting shear area. Due to the shape of notch and hollow shear pins easily to manufacture, both shear pin was studied in this regard as shown in Fig. 3. The steady outside diameter of both shear pins of 20 mm, which was equal to the original clevis pin, was observed. The notch depth of the notch shear pin was also varied from 1 to 19 mm, whilst hole diameter of the hollow shear pin was also considered from 1 to 19 mm.

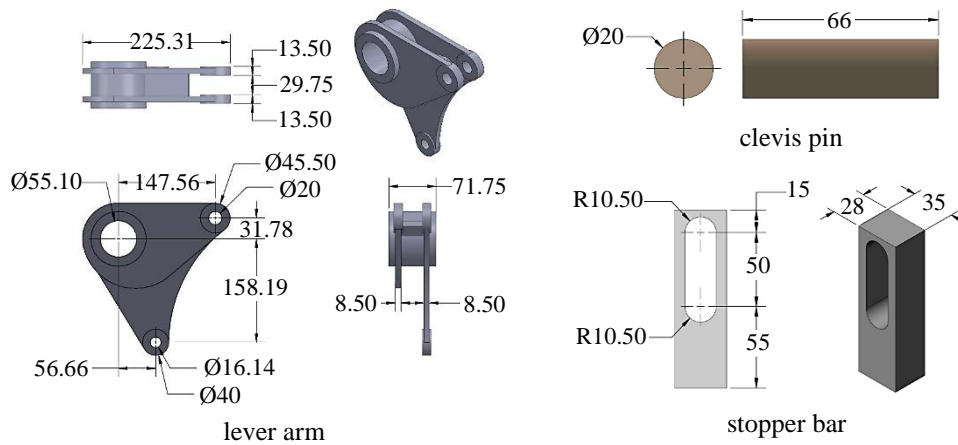


Fig. 2. The 3D model of the lever arm, clevis pin, stopper bar, and drawing in which all dimensions are in millimeters.

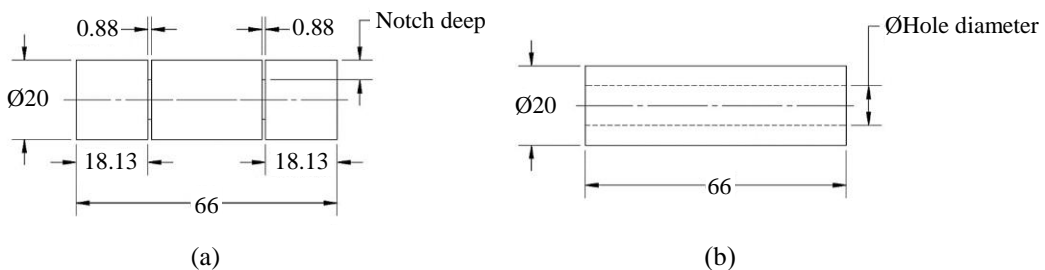


Fig. 3. The 3D model of (a) the notch shear pin and (b) the hollow shear pin drawing in which all dimensions are in millimetres.

2.2 Simulation Assembly Model

Fig. 4 shows the simulation assembly model, consisting of three main parts the lever arm, the clevis pin, and the stopper bar. The clevis pin was assembled into the holes at the end of the lever arm. The stopper bar was placed at an angle of 90 degrees with the axis of the lever arm and aligned with the center of the pin. The lever arm and the clevis pin, which are the moving parts, and the stopper bar was assigned as an impact abortion part. The initial gap between

the stopper bar and the pin was 2 mm. The angular velocity of the lever arm during the rotation is needed to simulate the impact between the clevis pin attached to the end of the lever arm and the stopper bar. Fig. 5 displays the installation of the Novotechnik IP6501 rotary sensor at the rotation axis of the lever arm. A Megger TM1800 circuit breaker analyzer and Wies SA100 switchgear analyzer were used to record and analyze the angular position at any moment of the lever arm. Based on the failure investigation, the fracture of the lever arm occurs during an opening circuit period. Fig. 6 illustrates the relation between angular position and time during the opening circuit. With respect to the kinematics of the mechanism, the impact occurred at the position 2 as shown in Fig. 6, which shows the angular velocity of 50 rad/s. This angular velocity was then set as the initial rotation velocity of the impact simulation.

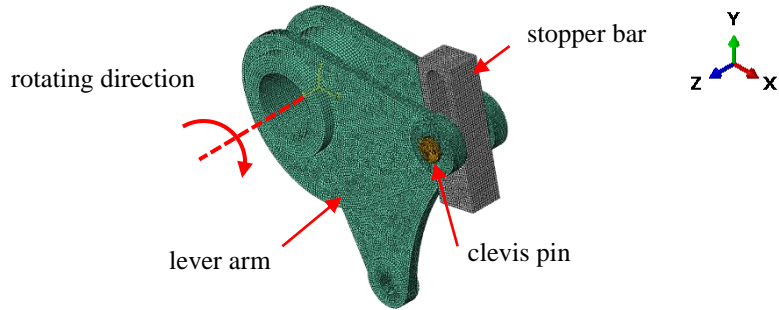


Fig. 4. The mesh and the assembly of the 3D models are used for simulating the impact.

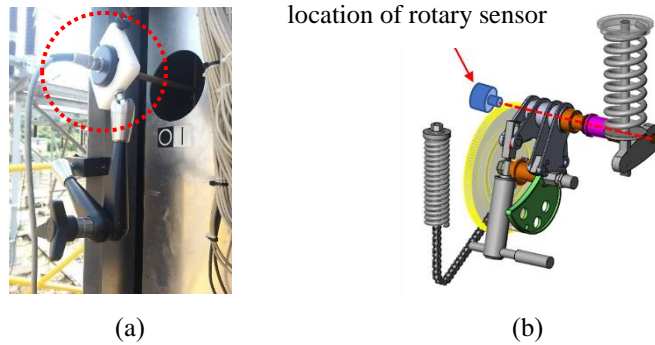


Fig. 5. (a) The rotary sensor for measurement of the angular displacement of the lever arm and (b) its installation position.

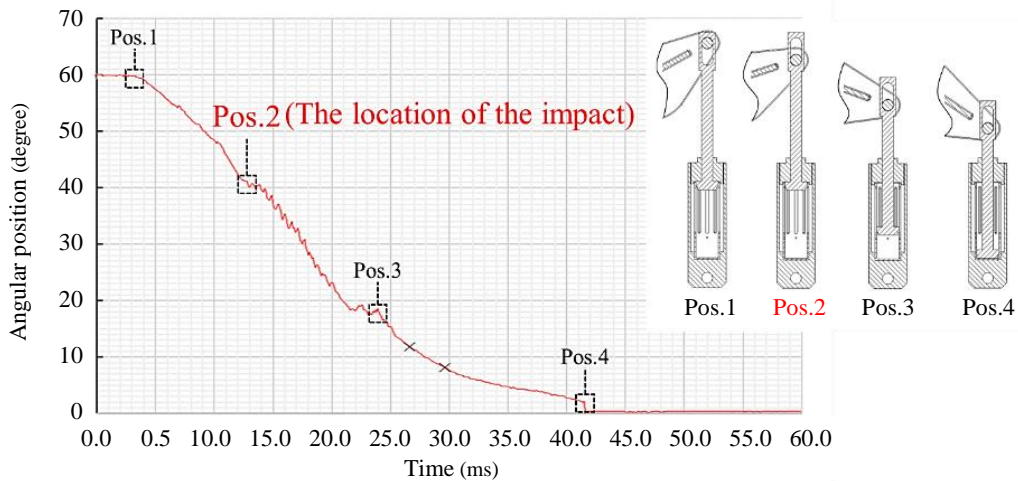


Fig. 6. The Angular position and time curve of the lever arm used for the calculation.

2.3 Material Properties and Mechanical Behavior Model

The materials of the lever arm and clevis pin are A356 sand cast aluminum alloy and AISI 420 martensitic stainless steel respectively, due to their unique mechanical properties [12, 13]. Their isotropic elastic properties are shown in Table 1. To explain the plastic properties, A Johnson–Cook model is calculated according to the following eq. 1 [10]:

$$\sigma = (A + B\varepsilon_p^n)(1 + C \ln \frac{\dot{\varepsilon}_p}{\dot{\varepsilon}_r}) \quad (1)$$

where σ (MPa) is flow stress, A (MPa) is the yield strength at the reference strain rate, B (MPa) is the strain hardening coefficient, C is strain rate hardening coefficient, n is strain hardening index, ε_p is equivalent plastic strain, $\dot{\varepsilon}_p$ (s^{-1}) is equivalent plastic strain rate, and $\dot{\varepsilon}_r$ (s^{-1}) is the reference plastic strain rate. The Johnson-Cook constitutive model parameters of A356 sand cast aluminum alloy and AISI 420 martensitic stainless steel are illustrated in Table 2, corresponding to the dynamic behaviours of strain hardening and thermal softening of the metal materials. These parameters are brought from previous report [14, 15].

According to literatures, the fracture process causes a large deformation and damage to the materials. To simulate the fracture process of the structure, a reasonable and effective damage model is critical. The stress-strain diagrams of both materials undergoing damage are shown in Fig. 7, suggesting a clear division of stages. At the initial O-A section, the material deformation shows a linear elastic deformation. Then, the material enters the plastic yield stage with the strengthening of strain at A-B stage. After that, at B-C section, the notably decreasing capacity of the material is then observed until fracture. At point B, thus suggests the starting of material damage, which is also known as the standard of damage beginning. After point B, the stress-strain behavior is examined by the progress of stiffness weakening in the local deformation period.

Based on the stress-strain behaviors of A356 and AISI 420, the simulation of the damage evolution was conducted using the Abaqus ductile damage model, including the softening of the yield stress and degradation of the elasticity. This damage model specifies that the damage initiates when plastic deformation reaches its limit. The model is utilized integrated with the Johnson-Cook material behavior model. According to the ASM Handbook Volume 2 [16], the plastic strain at initiation of damage (ε_0) of A356 was fixed as 0.035. In case of AISI 420, it was set as 0.12 based on the specimen tensile experiments [17]. Those suggest the beginning of the material damage. The complete loss of material bearing capacity is a main factor for material failure, which can define by the displacement of damage evolution. The past displacement limits of the deformation of elements are excluded from the simulations. This suggests gap openings within structures, corresponding to the expanded crack behaviors in the structure. The displacement limit can be calculated by multiplying the characteristic length of the mesh with the equivalent failure strain (ε_f). Based on the specimen tensile experiments and material elongations, the equivalent failure strain can be considered. The elongation of AISI 420 was 0.23 [17]. The tensile test specimens of a A356 Material were suddenly broken into two pieces without evident signs of necking deformation [18], indicating the same point of the equivalent plastic strain at the beginning of the material damage and equivalent failure strain. This led to the displacement damage evolution of A356 material assumed as zero.

Table 1: Material properties.

	Mass density (Kg/m ³)	Young's modulus (GPa)	Poisson's ratio
A356	2700	70	0.33
AISI 420	7800	200	0.30

Table 2: Johnson–Cook model parameter for A356 and AISI 420.

Materials	A (MPa)	B (MPa)	n	C
A356	270	155	0.28	0.018
AISI 420	450	738	0.388	0.02

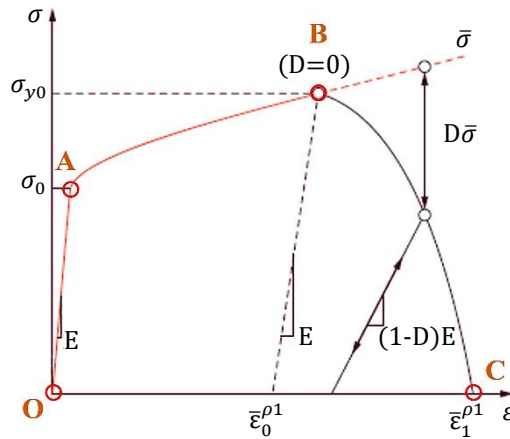


Fig. 7. Stress-strain relationship of metallic material.

2.4 Finite Element Model

The explicit nonlinear 3D finite element was selected to develop a full-scale 3D finite element model. The lever arm and clevis pin model were conducted by using a mesh of hexahedron elements with one integration point (C3D8R). In case of the stopper bar, it is not necessary to analyze the stress distribution. The stopper bar was modelled using a mesh of discrete rigid body elements (R3D4). The mesh element size of the lever arm, clevis pin, and stopper bar were fixed as 2 mm, 0.5 mm, and 2 mm, respectively. The finite element model was discretized as 298,074 nodes and 273,644 elements. The 3D finite element model with the mesh is shown in Fig. 4. Considering the contact that may occur during impact process of the structure, the surface-to-surface contact was assigned to be the contact between outer element of pins and inner element of lever arm's hole, involving a calculation of contact force. The surface of the inner hole is set as the master surface. The outer pin surface are slave nodes. The friction coefficients in the contact interfaces were 0.2 [19]. A hard contact algorithm was then adopted to prevent any penetration of slave nodes into the master surfaces. For the contact between pin and stopper bar, the general contact was used in the numerical simulation model. The boundary condition of the lever arm's model was assigned as only rotating in clockwise direction along the main hole of the lever arm. The pin was assembled into the holes at the end of the lever arm. Both part rotating with initial angular velocity of 50 rad/s. The stopper bar was impact abortion part. The bottom end of stopper bar was restrained in all degrees of freedom. The study of mesh size of pin and determination of its relationship with contact force is an initial part for development of analysis model. The mesh size is certainly related to the deviation's degree of the analyzed results from the actual situation. In the finite element model, the mesh size of clevis pin was slightly reduced from 3 mm in steps of 0.1 mm to determine the relationship between mesh size and contact force. Fig. 8 shows the contact force between the lever arm and clevis pin when the mesh size changes. For the decreasing of the mesh size, the contact force gradually increases and then stabilizes. As the mesh sizes smaller than 0.8 mm, it gently converges. Based on the result, the mesh size of 0.5 mm was then used in our analysis.

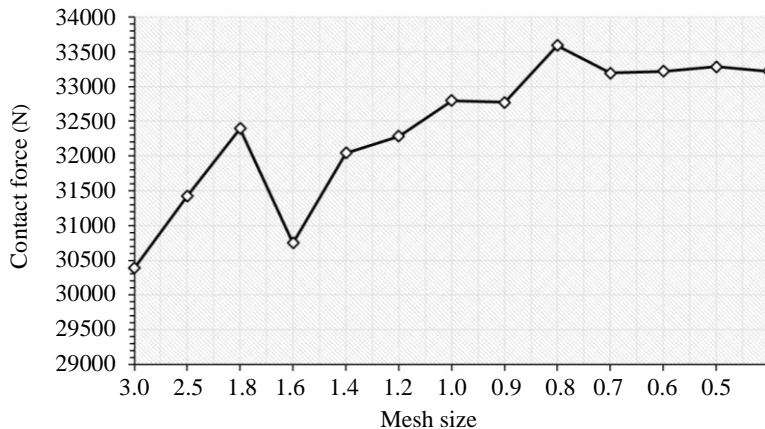


Fig. 8. Relationship between mesh size and contact force.

3. Results and Discussions

3.1 Determination of Failure Load of Shear Pin

The simulated results of the impact of the lever arm and clevis pin indicated the highest stress concentration and fracture located at the pinhole on the end of the lever arm (Fig. 9a), corresponding to the actual damage (Fig. 9b). To analyze a force from impact on the lever arm, in this research, the fracture load of the lever arm was calculated using the maximum value of the contact force between the pins and the lever arm's hole in the time-history curves as shown in Fig. 10. Moreover, the contact force curve between the shear pin and lever arm was demonstrated and the peak value was taken as the failure load. The failure load of the shear pin was also used to determine its fracture load in the design of the structural separation of the shear pin. From the simulated results of the lever arm and the clevis pin, the lever arm's fracture load or maximum contact load of 84,840 N (point C, Fig. 7), causing the fractured lever arm, was reported. However, the major role of the shear pin is a break-away part to protect damage on the lever arm. Therefore, the lever arm's fracture load of 84,840 N should not be a criterion for design the failure load of shear pin due to the strength of the shear pin as high as the strength of the lever arm. In this case, the lever arm may also be damaged due to the overload.

To prevent damage the lever arm by only breaking the shear pin, the failure load of the shear pin should be lower than the point A of Fig. 7. This point indicated the initial load of the plastic deformation of the lever arm. Therefore, the reduced impact rotating velocity was simulated, resulting in the appropriated velocity of 45 rad/s. This value led to the contact force of 32,680 N, corresponding to the retained equivalent plastic strain (PEEQ) of 0. Then, the limitation value of the shear pin's failure load was depended on the maximum contact force of 32,680 N.

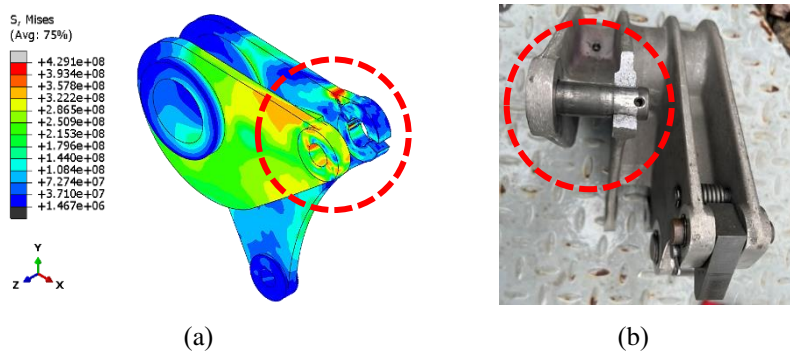


Fig. 9. (a) The location of the fracture and the stress distribution on the lever arm from the simulation result and (b) the location of the actual fracture on the lever arm.

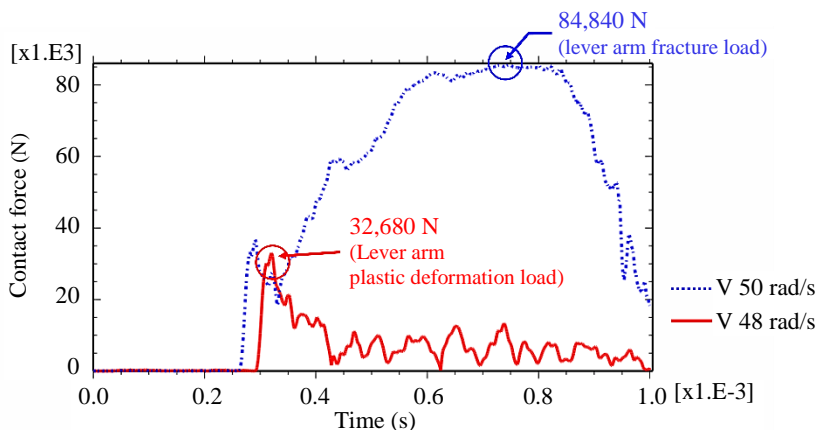


Fig. 10. Illustration of the fracture load and initial plastic deformation of the lever arm from the history time versus the contract force between the pins and the lever arm's hole.

3.2 Finite Element Analysis of Shear Pin

The prominent aspect of the current work is the study of the substitutability of a clevis pin with a shear pin. The impact of the notch pin and the hollow pin were simulated to analyze the failure load in the fracture processes. The failure load of the shear pin from the peak of contact force was calculated using the same procedure as the fracture load on the lever arm. The failure load of the shear pin with different notch depths and inner diameters were shown in Fig. 11. The notch pin with 6 mm in depth and the hollow pin with an I.D. of 17 mm were the highest failure load on the pin, which were less than the initial plastic deformation of the lever arm. The structural deformations and stress distributions of both pins after impact are shown in Fig. 12. In the initial process, the shear pin was affected by an impact load, resulting in stress concentration at the notch surface. The plastic strain was subsequently accumulated in the pin structure. The stress concentration part reached the plastic strain limit, leading to the initiation of damage accompanied by cracks. Finally, the crack of the pin structure intersected. Then, the shear pin was completely fractured.

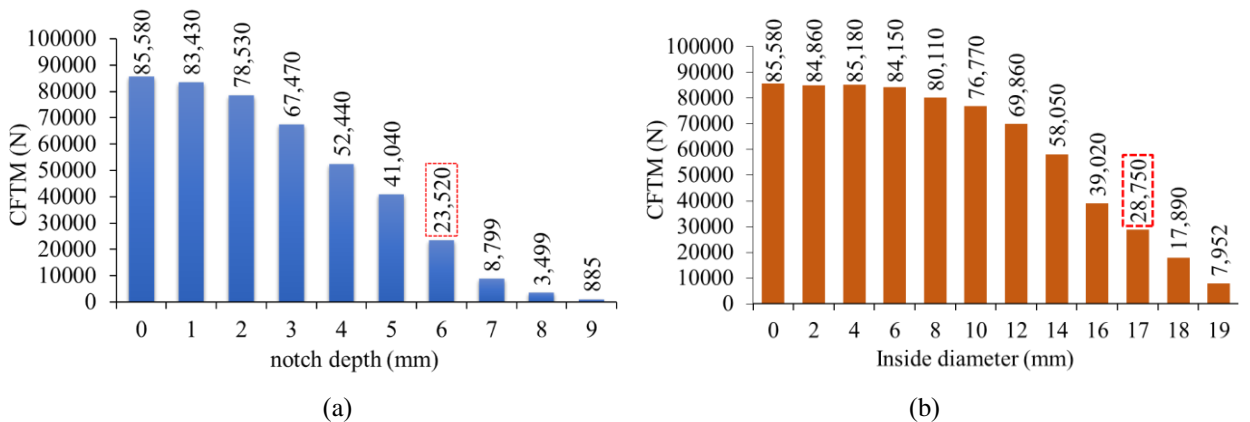


Fig. 11. Peak of contact force on lever arm (CFTM) when simulated with different size of (a) notch pin and (b) hollow pin.

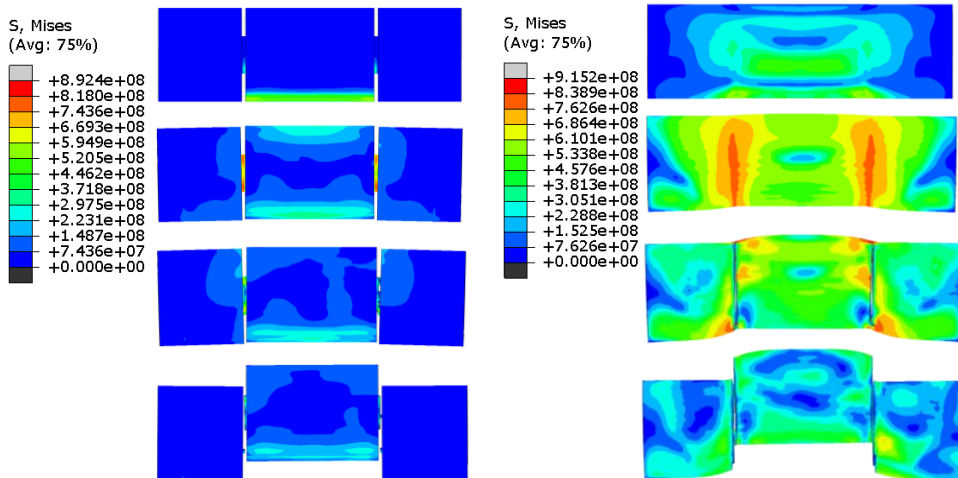


Fig. 12. Simulation of the failure process of the notch and hollow shear pins.

Table 3 and Table 4 suggest the dependence of failure load and fracture energy on the shear cross-sectional area. When the shear cross-sectional area decreased, failure load and fracture energy were also decreased. By only using the notch pin with 6 mm in depth, there was no plastic deformation of the lever arm. In case of the hollow pin, the failure load of 32,680 N according to the impact of the lever arm should not be considered for size selection. Considering the similar shear cross-sectional area of both pins, *i.e.* 28.27 mm² (notch pin with 7 mm in depth) and 30.63 mm² (hollow pin with I.D. of 19 mm), their failure loads were comparable. While the dissipation energy of the

notch pin was significantly low. The notch has induced a significant change in the maximum shear stresses on the pin. Owing to profound effect of the notch, it plays a crucial role for localizing stress and increasing stress concentration [20]. The impact loads normally fracture the notch pin with more susceptible due to the impulse of the force, resulting in a short duration in fracture process. With respect to the higher energy dissipation of the hollow shear pin, the fracture process was prolonged due to a decreased overall stiffness by increasing of inner diameter. This generated a large plastic deformation before the fracture began. Therefore, the use of the notch pin with 6 mm in depth should be highly suitable for being the shear pin for preventing damage on the lever arm.

Table 3: Notch depth, shear cross-section area, failure load, dissipation energy of notch shear pin, and lever arm equivalent plastic strain (PEEQ).

Notch depth (mm)	Shear cross-section area (mm ²)	Pin failure load (N)	Dissipation energy (J)	Lever arm PEEQ
9	3.14	885	7.44	0.0000
8	12.57	3499	8.15	0.0000
7	28.27	8799	13.46	0.0000
6	50.27	23520	37.68	0.0000
5	78.54	41040	79.15	0.0215
4	113.10	52440	114.95	0.0329
3	153.94	67470	192.22	0.0553

Table 4: Inner diameter, shear cross-section area, failure load, dissipation energy of hollow shear pin, and lever arm equivalent plastic strain (PEEQ).

I.D. (mm)	Shear cross-section area (mm ²)	Pin failure load (N)	Dissipation energy (J)	Lever arm PEEQ
10	235.62	76770	419.44	0.5295
12	201.06	69860	261.57	0.9697
14	160.22	58050	182.56	0.1026
16	113.10	39020	120.10	0.0917
17	87.18	28750	100.73	0.0879
18	59.69	17890	63.70	0.0524
19	30.63	7952	34.76	0.0010

4. Conclusion

Herein, the design and analysis of the shear pin to prevent the fracture on the lever arm caused by impact inside the circuit breaker mechanism. The simulation of the impact on the lever arm was conducted by using the explicit finite element method to determine a load on the lever arm. The initial plastic deformation load of the lever arm, which was the highest force on the lever arm without any damage, could be a criterion for the investigation of the failure load of the shear pin. The notch and hollow shear pins were also simulated by using the same finite simulation model with different notch- depths and I.D.-widths. Based on the simulation, the failure load of the notch pin with 6 mm in depth and the hollow pin with I.D. of 17 mm was similar value as the initial plastic deformation load of the lever arm. The notch pin could prevent a damage on the lever arm due to the increased stress concentration on the pin's surface and low dissipation energy, leading to easier break-away after impact. On the other hand, the hollow pin, which had the failure load lower than the initial plastic deformation load of the lever arm, could not protect the lever arm. This might be due to the large deformation of the hollow pin, resulting in the high dissipation energy. Consequently, the hollow pin could not be a good break-away device. Considering only the initial plastic deformation load of the lever arm to predict the suitable size of the hollow pin might be not a good criterion. The dissipation energy was also critical. Based on the results, the notch pin with 6 mm in depth was, therefore, a better candidate to be a break-away part for protecting the lever arm.

Acknowledgments

This work was funded by the Electricity Generating of Thailand and supported by Chiang Mai University and National Metal and Materials Technology Center (MTEC).

References

- [1] Dufournet D. AC high-voltage circuit breakers. Maine: IEEE; 2017.
- [2] Alstom Company. Instruction manual of SF6 circuit breaker XFT1 5 - FXT1 6 with spring operation mechanisms FK3-4. Paris: Alstom Company; 2000.
- [3] GE Grid. Backgrounder of technical improvement to FK3-4/127 and FK3-5/127 spring operating mechanisms. Oberentfelden: GE Grid; 2016.
- [4] Boonsong C, Nithinuna K. The root cause failure analysis (RCFA) of broken lever problems of 230 kV circuit breaker for power generation. Nonthaburi: Electricity Generating Authority of Thailand; 2012. (In Thai)
- [5] Kiran Kumar BS, Venkata Rama Reddy M, Kumar K. Pin shear –material testing and validation using finite element analysis (ANSYS). *Int J Eng Res Technol*. 2015;4(7):165-170.
- [6] Budiman BA, Suharto D, Djodikusumo I, Aziz M, Juangsa FB. Fail-safe design and analysis for the guide vane of a hydro turbine. *Adv Mech Eng*. 2016;8(7):1-8.
- [7] Sankar S, Nataraj M, Prabhu Raja V. Failure analysis of shear pins in wind turbine generator. *Eng Fail Anal*. 2011;18(1):325-339.
- [8] Yu M, Zhang P, Xue C. Diameter-thickness ratio influence on large civil aircraft fuse pins' strength. *J Phys Conf Ser*. 2022;2368:012029.
- [9] Hiremath S, Chiniwar DS, Singh Z, Behera A, Saxena KK, Vishwanatha HM. Modelling and simulation of lightweight hollow pins as a substitution for solid shear pins used for assembly joints in aerospace applications. *Int J Interact Des Manuf*. 2023;17:2593-2606.
- [10] Zhang P, Nie H, Wu J, Yu M. Emergency separation simulation and damage Prediction of an airliner under wheel-up landing condition. *Shock Vib*. 2021;2021:1-19.
- [11] Jin Z, Zhou J, Li D. Finite element simulations of dynamic shear fracture of shear pins. *Int J Aerosp Eng*. 2021;2021:1-16.
- [12] Kaufman JG, Rooy EL. Aluminum alloy castings: properties, processes, and applications. USA: ASM International; 2004.
- [13] Brnic J, Turkalj G, Canadija M, Lanc D, Krscanski S. Martensitic stainless steel AISI 420 mechanical properties, creep and fracture toughness. *Mech Time-Depend Mater*. 2011;15:341-352.
- [14] Gupta S, Abotula S, Shukla A. Determination of Johnson-Cook parameters for cast aluminum alloys. *J Eng Mater Technol*. 2014;136(3):034502.
- [15] Korkmaz ME, Günay M. Finite element modelling of cutting forces and power consumption in turning of AISI 420 martensitic stainless steel. *Arab J Sci Eng*. 2018;43:4863-4870.
- [16] Zwilsky KM, Langer EL. Properties and selection: nonferrous alloys and special-purpose materials. USA: ASM International; 1990.
- [17] Ulas HB, Ozkan MT. Turning processes investigation of materials austenitic, martensitic and duplex stainless steels and prediction of cutting forces using artificial neural network (ANN) techniques. *Indian J Eng Mater Sci*. 2019;26:93-104.
- [18] Mae H, Teng X, Bai Y, Wierzbicki T. Comparison of ductile fracture properties of aluminum castings: sand mold vs. metal mold. *Int J Solids Struct*. 2008;45(5):1430-1444.
- [19] Mahdavian SM, Mai YW, Cotterel B. Friction, metallic transfer and debris analysis of sliding surfaces. *Wear* 1982;82(2):221-232.
- [20] Budynas RG, Nisbett JK. Shigley's Mechanical Engineering Design. 10th ed. New York: McGraw-Hill Education; 2015.